A Modular Bio-Platform Based on a Versatile Supramolecular Multi-Enzyme Complex Directly Attached to Graphene

Abeer Alshammari[1,2,3‡], Mareike G. Posner[1,4‡], Abhishek Upadhyay[1,4], Frank Marken[5], Stefan Bagby[1,4], and Adelina Ilie[1,2]**

[1] Centre for Graphene Science, University of Bath, Bath, BA2 7AY, UK

[2] Department of Physics, University of Bath, Bath, BA2 7AY, UK

[3] Department of Physics, King Saud University, Riyadh 11451, Saudi Arabia

[4] Department of Biology and Biochemistry, University of Bath, Bath, BA2 7AY, UK

[5] Department of Chemistry, University of Bath, Bath, BA2 7AY, UK

Keywords: graphene; supramolecular dihydrolipoyl acyltransferase complexes; biosensing; functional hybrid interfaces; E2 complexes

Abstract

Developing generic strategies for building adaptable or multi-functional bio-platforms is challenging, in particular because protein immobilization onto surfaces often causes loss of protein function and multi-functionality usually necessitates specific combinations of heterogeneous

elements. Here we introduce a generic, modular bio-platform construction strategy that uses cage-like supramolecular multi-enzyme complexes as highly adaptable building blocks immobilized directly and non-covalently on graphene. *Thermoplasma acidophilum* dihydrolipoyl acyltransferase (E2) supramolecular complexes organize as a monolayer or can be controllably transferred onto graphene, preserving their supramolecular form with specific molecular recognition capability and capacity for engineering multi-functionality. This E2-graphene platform can bind enzymes (here, E1, E2's physiological partner) without loss of enzyme function; in this test case, E1 catalytic activity was detected on E2-graphene over six orders of magnitude in substrate concentration. The E2-graphene platform can be multiplexed via patterned co-transfer of differently modified E2 complexes. As the E2 complexes are robust and highly customizable, E2-graphene is a platform onto which multiple functionalities can be built.

1. Introduction

Flexible and unified strategies for tailoring a variety of functions on a single bio-platform are highly desirable. Multi-functionality is usually built in by non-generic combination of heterogeneous elements.[1] One generic approach used non-covalent functionalization of sensing platforms,[2,3] nanostructures[4] and nanomaterials[4,5] with peptides selected from combinatorial libraries. Supramolecular bio-complexes, however, could provide multi-functionality with adaptable biorecognition in fewer steps. Biomolecular nanoscale architectures on surfaces have been exploited or created for biosensing, biocatalysis, biofuel cells and biobatteries[6-9]. These have often used a synthetic or natural polymer scaffold,[10,11] including synthetic protein scaffolds[12] or inorganic nanoparticles[13] to allow immobilization or embedding of biomacromolecules or organelles with functional retention or enhancement.

Since its outstanding sensitivity to chemical functionalization was demonstrated,[14] graphene has been investigated for sensing chemical and biological analytes.[15-17] As for carbon nanotubes, non-covalent functionalization allows preservation of graphene's electronic properties[18] and is thus beneficial for sensor design. Numerous approaches have been used to so functionalize graphene. Peptides screened for graphene binding[19,20] were linked to anti-microbial peptides that bind bacterial pathogens,[21] or used to detect streptavidin against a background of bovine serum albumin.[22] Tripodal NHS-esters were designed to π-stack on graphene and create protein conformation-preserving interfaces.[23,24] Photosystem I (PSI), a very large, polar supercomplex, was immobilized on a polycyclic aromatic compound-modified graphene interface;[25] controlling PSI orientation relative to the functionalized graphene surface allowed better electrochemical communication with the electrode. Studies of non-covalent graphene functionalization with DNA include DNA aptamer-based sensors.[26] Other examples involve host–guest supramolecular interactions[27,28] and acetylcholinesterase covalently grafted to polymer brushes.[29] Direct graphene functionalization with protein is less common, but one notable example is the hydrophobins, amphipathic fungal proteins that form a monolayer on graphene.[30]

Here we show that the versatile and robust central scaffold of naturally occurring supramolecular multi-enzyme 2-oxoacid dehydrogenase complexes (OADHCs)[31,32] can be immobilized directly on graphene to create a versatile platform for sensing or other applications. OADHCs are composed of multiple copies of three enzymes: E1 (2-oxoacid decarboxylase), E2 (dihydrolipoyl acyltransferase) and E3 (dihydrolipoamide dehydrogenase). An E2 monomer comprises N-terminal lipoyl domain (E2lipD), peripheral subunit binding domain (PSBD) and catalytic acyltransferase domain (Figure 1).[31] Multiple copies of the E2 acyltransferase domain assemble to form the core scaffold of OADHCs. E1 and E3 assemble around this E2 core scaffold via non-

covalent protein-protein interactions; E1 and E3 bind specifically and mutually exclusively to the PSBD of E2[33,34] (Figure 1). The E2 core scaffold is a naturally occurring cage-like protein supramolecular complex composed of E2 trimers at each vertex of a polyhedron to give a total of 24, 42 or 60 E2 monomers, depending on the particular complex and source organism.[35,36]

We use the E2 protein supramolecular complex from *Thermoplasma acidophilum* (*T. acidophilum*), a thermophilic archaeon, to bio-functionalize graphene directly, without a π–π stacking agent or other chemical linker. The strength of, and rationale for, this approach arise from the following characteristics of E2 supramolecular complexes: E2 complexes assemble reproducibly from E2 monomers;[32,35] E2 complexes have excellent production and handling properties e.g. *T. acidophilum* E2 complexes are stable up to 60 ºC;[37] E2 complex symmetry means that controlling orientation on graphene is much less critical than it would be for most proteins; E2 complexes have both exterior and interior surfaces, so can be used as scaffolds,[38,39] cages/capsules[40,41] or reaction vessels,[42] or a combination of these;[43] by fusing the catalytic acyltransferase domain (Figure 1) with (poly)peptides other than E2lipD and PSBD, an E2 complex can be assembled from a mixture of different monomers;[44] the functionality of the interior and exterior surfaces can be post-translationally manipulated, for example by introducing non-native surface cysteines for functionalization[45] or by exploiting sortase A to decorate the E2 complex exterior with multiple functional entities;[38,39] and E2 complexes can be converted to molecular switches via site directed amino acid changes that make complex assembly responsive to external conditions such as pH.[46,47] E2 complexes are therefore highly customizable and can be rendered multi-functional. These properties combined make E2 complexes suitable vehicles for biotechnological, therapeutic, and diagnostic applications. If E2 complex functionality can be

preserved while interfaced with the solid state, moreover, as we demonstrate here, E2 complexes can become a generic template for incorporation into bio-platforms of multiple recognition/binding or catalytic elements, for example, promising single-platform multi-functionality.

Here we have created a modular E2 complex-functionalized graphene platform, and demonstrated its viability for sensing through partner enzyme (E1) binding and activity measurement; E1 alone did not show any activity on bare graphene. This is also the first structural study of E2 complexes interfaced with the solid state: combined information from atomic force and transmission electronic microscopies (AFM and TEM) shows that E2 complexes retain a supramolecular structure upon direct adsorption onto graphenic surfaces. Graphene obtained by chemical vapor deposition (CVD),[48] a thin film material of interest for many practical electronic[48] and bioelectronics devices,[17,21,49] emerges as a suitable solid state interface for E2, offering assembly opportunities and facilitating electron transfer. Finally, we have also shown transfer of different variants of E2 complexes onto graphene as a first step towards creation of multiplexed, multi-functional devices.

2. Results and Discussion

2.1. E2 complex synthesis and characteristics

Full length *T. acidophilum* E2, including catalytic and peripheral domains (Figure 1), was obtained in its monomeric form as previously described (see Supporting Information – SI – Figure S1).[37] *T. acidophilum* E2 complex assembly is temperature driven.[37] Assembly at 55 °C resulted in predominantly 60-mer E2 complexes (see below and SI, Figure S3): 60 copies of E2 acyltransferase domain self-assemble to form the OADHC core, each E2 also providing an E2lipD

and a PSBD which are arranged around the core. E2 trimers assemble in the corners of a dodecahedron giving icosahedral symmetry[35] (Figure 1). Once assembled, the E2 supramolecular complexes are stable for at least a week if stored at 4 °C in PBS, as is purified E2 partner enzyme E1.

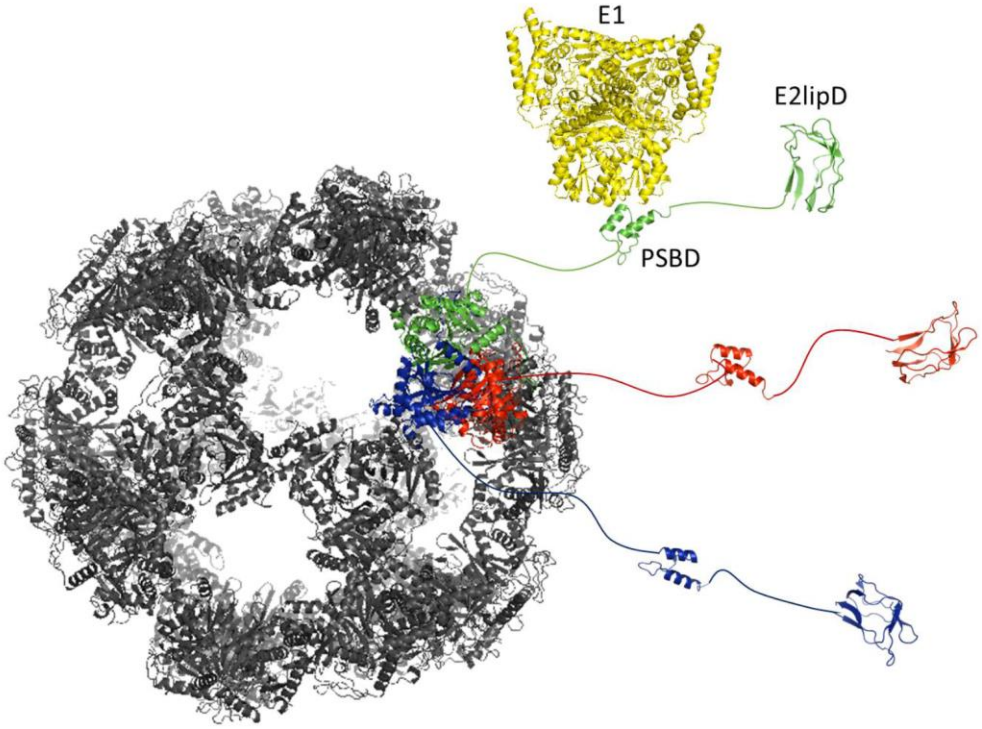

Figure 1. Schematic structure of the catalytic core of a 60-mer E2 complex. The catalytic domains of E2 monomers can assemble into dodecahedral (60-mer)[31] or cubic (24-mer; not shown here)[31] or oblate spheroid (42-mer; not shown here)[36] complexes. In an E2 60-mer, trimers of the E2 catalytic domain occupy each corner of the dodecahedron (E2 monomers making up one trimer are shown in green, red and blue). The peripheral subunit binding domain (PSBD) and E2 lipoyl domain (E2lipD) of each E2 monomer extend from the catalytic core via unstructured linkers (linkers not shown to scale). A molecule of E1 (yellow), the natural binding partner of E2, can bind to each PSBD on the E2 complex (for simplicity, only one E1 molecule is shown).

2.2. Interfacing E2 with graphene: structural characterization

When building the platform comprising E2 complexes immobilized on graphene, henceforth termed E2-graphene, we were interested in characteristics that can affect platform performance. Is E2 complex supramolecular structure preserved while interacting with graphene? What is the nature and strength of this interaction? Do E2 complexes create monolayers? What is the protein uptake on graphene, and can this be controlled?

To address these questions, we compared adsorption, assembly on surfaces and structural changes of E2 complexes interfaced with several graphene-based substrates: (i) CVD graphene; (ii) atomically flat, basal plane highly oriented pyrolytic graphite (HOPG); and (iii) single- or few-layer graphene (FLG) flakes obtained through mechanical exfoliation of graphite[50] (of, typically, tens of microns in lateral size), with smoothness intermediate between HOPG and CVD graphene. Both CVD graphene and FLG flakes were supported on SiO_2/Si substrates. In order to reveal adsorption/assembly characteristics and high resolution morphology of immobilized E2, we used atomic force microscopy (AFM) operated in tapping mode at low forces[51,52] (Experimental Section and SI), in air and liquid, and in both imaging and spectroscopic modes. AFM was supplemented by TEM of E2 complexes supported by CVD graphene membranes, with corroboration from images of individual complexes in frozen solution by cryo-EM (SI, Figure S3).

Of primary interest for applications was large area, high throughput CVD-grown graphene: it is suitable for cost-effective sensor production (including flexible substrates),[48,49] can be transferred cleanly onto insulating surfaces, and offers adequate performance as an electrode relative to carbon-based electrodes.[53] In terms of suitability for E2 complex solid state interfacing, we

expected CVD graphene to resemble basal plane HOPG, a substrate routinely used for molecular self-assembly; HOPG, in contrast to CVD graphene, is a poor electrode.[54]

E2 complex uptake on graphenic surfaces *via* direct, non-covalent attachment

For structural investigation, E2 complexes were transferred onto the aforementioned graphene surfaces using filter paper drying: E2-incubated surfaces were dried by turning the sample upside down with only the water meniscus allowed to come into contact with filter paper. This resulted in broadly reproducible percentage coverage with protein uptake controlled by varying concentration/adsorption time, and isolated complexes at low coverage (Figure 2) which could be reliably investigated by AFM in air. Alternatively, samples were not allowed to dry, surface attachment taking place directly from liquid. This complementary air/liquid approach for high resolution AFM structural investigations was used due to insufficient immobilization of individual E2 complexes for AFM scanning in liquid (see SI).

After transfer of E2 complexes by filter paper drying, hydrophobic HOPG and FLG flake surfaces became highly hydrophilic. On HOPG (Figure 2(a)) and CVD graphene (Figure 2(b)), individual complexes could be identified as dome-like structures, with internal details visible in higher resolution images (Figure 3). We show only one example of sub-monolayer coverage on FLG flakes due to the larger variability in percentage coverage (Figure 2(c)); some coalescence of the E2 complexes occurred, which we attribute to confinement effects caused by the microscopic boundaries of the flake. Uptake on CVD graphene seemed slightly higher than on HOPG and FLG, possibly related to the presence at low density of hydrophilic groups on CVD graphene (SI, Figure S5). The resulting E2 complex monolayer had a higher degree of disorder than on HOPG or FLGs,

attributed to CVD graphene being slightly rougher than exfoliated FLGs (SI, Figure S6) due to different processing methods. Nevertheless, images at varying degrees of coverage indicate that stacking of E2 complexes does not occur; this is advantageous as such stacking could slow electron transfer to graphene during electrochemical sensing. Initially, a detailed comparison of supramolecular E2 with monomeric E2 on graphene was also planned. In contrast to supramolecular E2 complexes, however, E2 monomers clustered together and possibly stacked on graphenic surfaces, creating an inhomogeneous protein layer with highly uneven height profile and morphology (Figure S7). This showed that, in contrast to E2 complexes, there is less control over E2 monomer orientation, and creation of monolayers or layers with controlled thickness from them.

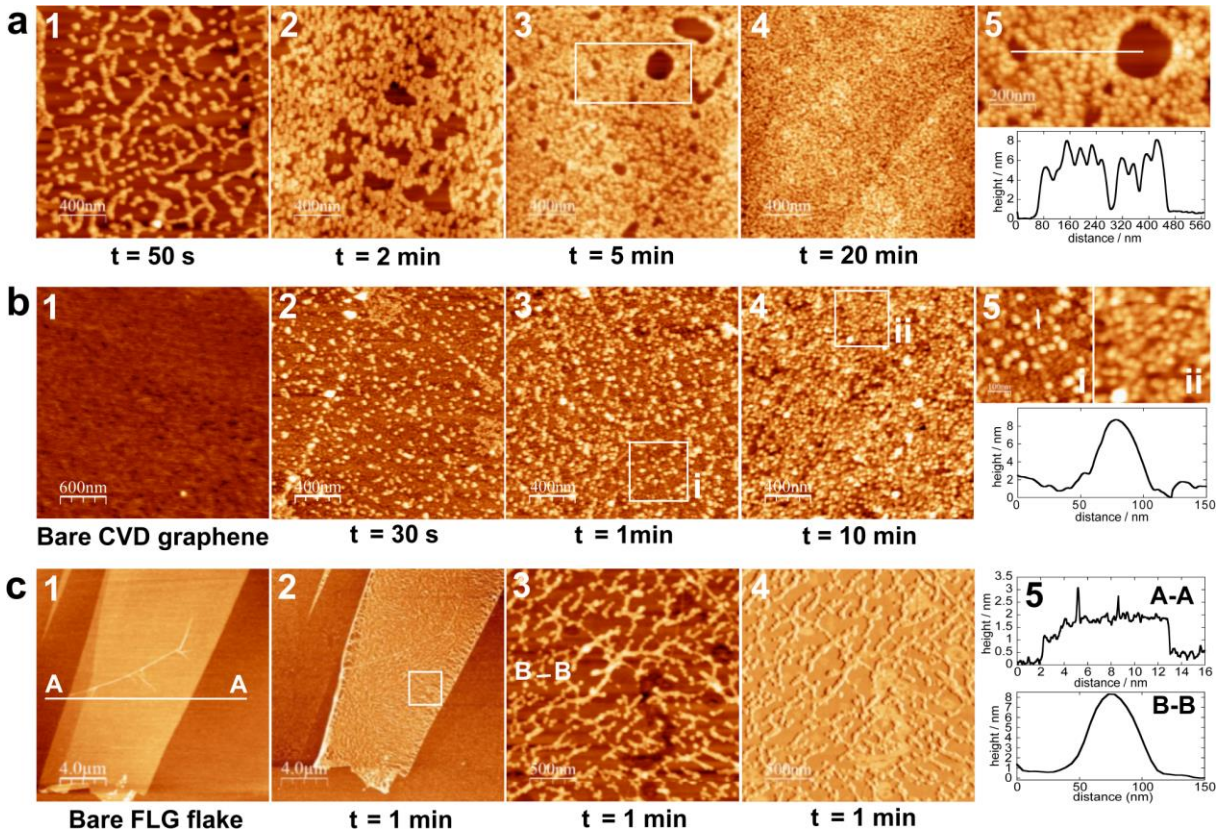

Figure 2. AFM topographic images of representative E2 complex coverage from filter paper drying on various graphenic surfaces. *Row (a): HOPG. Row (b): CVD graphene. Row (c): FLG flake.* Under each panel, the corresponding incubation time, t, is indicated. Individual complexes are clearly seen at sub-monolayer coverage on all surfaces. In each row, panel 5 shows details of framed regions from corresponding main images, with focus on the height profile of complexes on each of the three graphenic surfaces. Row (c) shows the topography of an FLG flake before and after E2 incubation, panels 1 and 2, respectively; panels 3 and 4 are topography and phase (for enhanced visibility of E2 complexes) images, of framed region from panel 2; panel 5 also shows the thickness of the bare graphene flake (line profile A-A).

Data acquired in liquid on samples that were never dried (Figure 3(c) and SI, Figure S9) confirm that no stacking of E2 complexes occurs by direct attachment, ensuring monolayer formation at complete coverage. E2 complexes adsorb onto graphenic surfaces *directly* from solution, pointing to interactions such as van der Waals and π-π interactions (as opposed to the mere drying process) as the trigger for their attachment. The process leads to monolayers (Figure 3(c), panel 2), showing that the complex-complex interaction while surrounded by buffer is too weak to cause stacking. The E2-graphene interaction while surrounded by liquid is relatively weak, as expected from non-specific, non-covalent interaction, such that the tapping AFM tip can swipe clean the surface at moderate scanning speeds (a few Hz/scanline) (SI, Figure S9). Graphene-supported E2 complexes are stable when immersed in PBS and two-fold diluted PBS, while they disintegrate if stored in pure water.

High resolution features of graphene-supported E2 complexes

High resolution imaging can inform about the extent to which E2 supramolecular structure is retained after attachment to graphene. TEM of E2, in dried state on CVD graphene membranes, and stained for contrast (Figure 3(a)), revealed polyhedral, cage-like, graphene-bound E2 complexes that are ~17 ± 0.8 nm across (less than ~22 nm as in structural models of *Bacillus stearothermophilus* pyruvate dehydrogenase, a 60-mer E2 complex,[32] possibly due to dehydration)[55], and somewhat poly-disperse overall. We observed two high symmetry orientations with five-fold and three-fold projections respectively (Figure 3(a) insets), which correlate well with supporting cryo-EM images of *T. acidophilum* 60-mer E2 (SI, Figure S3). High resolution AFM of graphene-supported individual E2 complexes and of assembled monolayers, in air (Figure 3(b)) and liquid (Figure 3(c)), revealed intra-cage details of individual E2 complexes. All these images show units with a "spokes-on-wheel" aspect; lobe-like components are arranged with five-fold symmetry around a central cavity (e.g. Figure 3(b)), consistent with the cryo-EM pentagon projection of the polyhedral cage (Figure S3). We assign the lobe-like units to the trimer assembly in the corners of the E2 polyhedron (Figure 1). The combined evidence points to 60-mer E2 as the predominant assembly in our samples. Figure 3(c), panel 2 shows the CVD graphene-bound E2 complexes while in buffer solution assembled in a compact, full layer: E2 complexes appear to preferentially show the "spokes-on-wheel" face, consistent with their pentagonal sides facing the viewer and, consequently, also the graphene substrate. A full monolayer of E2 complexes on graphene amounts to 1400 ng cm^{-2} approximately (see SI). We also note that in all AFM images (Figures 2 and 3), E2 complexes appear as near-identical units on a given surface. This would be difficult to maintain were the E2 complexes to undergo major loss of structure and indicates that the E2 complexes are robust to interfacing with graphene.

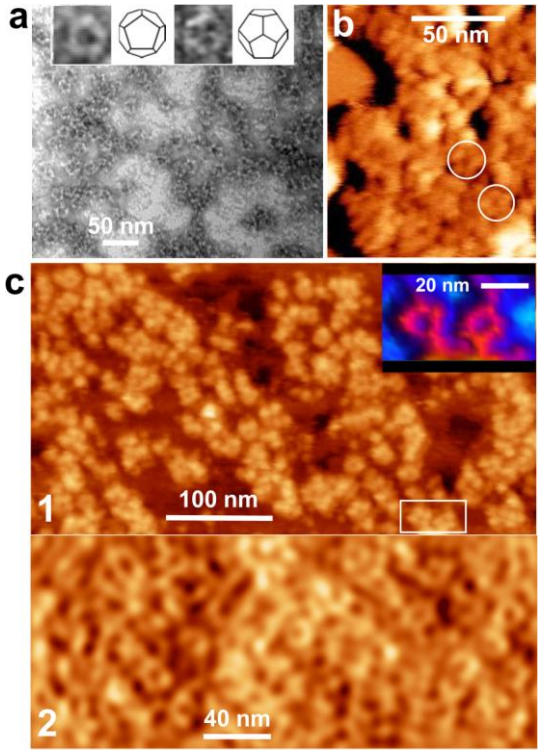

Figure 3. Structural details from TEM and high resolution AFM of E2 complexes adsorbed on CVD graphene. (a) TEM (at 100 keV) of dry, uranyl acetate-stained E2 complexes reveals the polyhedral structure of the E2 cage, with both five- and three-fold projections (see insets); to be compared with cryo-EM, Figure S3. (b) AFM phase image obtained in tapping mode in air, in a regime of attractive, non-compressive dynamic forces[51,52] on a partial E2 layer: within, five-lobe units (examples circled), consistent with the five-fold projection of the E2 complex polyhedral cage seen in TEM and cryo-EM. (c) Topographic images, tapping mode in liquid of individual complexes (c, panel 1), and complete self-assembled monolayers (c, panel 2). No protein fixation protocol was used (see SI).

E2 complex structural deformation upon interaction with hydrophobic and hydrophilic surfaces

The apparent, measured height after drying of E2 complexes (as obtained from tapping mode AFM in air operated in a regime of no compressive forces, see Experimental Section) on all graphene-based surfaces is 8-9 nm (Figure 2); corrections based on analysis of AFM spectroscopic curves led to real heights ~ 10-11 nm (SI, Figure S10), i.e. lower than the diameter of ~17 ± 0.8 nm that we observed in TEM. This demonstrates a significant compression of the hollow E2 complexes after drying on graphene-based surfaces. However, similar E2 complex heights were also obtained on HOPG functionalized with 1-pyrene butanoic acid succinimidyl ester (intended to prevent protein collapse)[56] which π-stacks on graphite and links covalently to protein surface NH_2 groups (SI, Figure S11), showing that such a linker strategy may not offer advantages over direct functionalization of graphene with E2 complexes. To put the E2 deformation on the hydrophobic graphene surfaces into a wider context, we compared it with the height of E2 complexes (adsorbed using same protocol) after drying on hydrophilic surfaces, such as SiO_2, a surface with a roughness around ~ 0.5 nm rms, and atomically flat sapphire (keeping in mind that the E2 complex surface offers both hydrophilic and hydrophobic sites for interaction, without any large clusters of positively or negatively charged side chains; SI, Figure S2). E2 complex height after drying on hydrophilic surfaces (SI, Figure S11) was ~4 nm, compared to 10-11 nm on graphenic ones. This is compatible with significantly stronger E2 complex interaction with hydrophilic surfaces, suggesting that graphene alters E2 complex conformation less than hydrophilic surfaces.

We also induced drying-mediated self-assembly of E2 complexes (by allowing a drop of liquid to dry in static air in a glovebox),[57] where not just mere adsorption from liquid onto surface takes place, but dynamic forces induced by the receding liquid front during drying drive the complexes

to move across the surface. E2 complexes organize on graphenic surfaces (CVD, mechanically exfoliated graphene, and HOPG) in network-, cellular-, and labyrinth-type patterns[58] that strikingly resemble those induced in colloidal complexes[57] (SI, Figure S8). Such patterns can form only if the E2 complexes have sufficient surface mobility,[57,59] proving that the graphenic surface-E2 complex interaction *at the liquid-solid interface* is weak. A weak interaction favors preservation of E2 complex supramolecular structure. In contrast, in similar experiments with a range of hydrophilic substrates (such as atomically flat sapphire and SiO_2), E2 complexes lacked mobility and did not form such patterns, remaining isolated (SI, Figure S8 (a)). This indicates that at the liquid-solid interface, E2-hydrophilic surface interaction is much stronger than E2-hydrophobic (graphenic) surface interaction, correlating with E2 complex height collapse while dry on hydrophilic surfaces.

Overall, both TEM and AFM evidence in liquid and in air, including high resolution features and surface assembly characteristics, corroborates that E2 largely retains its supramolecular structure on graphene; this is an important property for future utility of this first iteration of the E2-graphene bio-platform. Molecular dynamics (MD) simulations in explicit solvent indicate that like the E2 complex, immunoglobulin G (IgG) and bovine serum albumin retain their structures upon adsorption on graphene.[60,61] In the IgG case, the simulation results were supported by AFM images.[60] MD simulations suggest that IgG-graphene adsorption is dominated by van der Waals forces, and this is thought to be the case for graphene adsorption of large proteins more generally.[60] While van der Waals forces may also be prominent in E2 complex adsorption on graphene, contributions from other interactions such as π-π stacking cannot be ruled out. Analysis of the 3D structures of *T. acidophilum* E2lipD[62] and *Geobacillus stearothermophilus* PSBD-E1 complex[33]

suggests, for example, that in *T. acidophilum* E2 the side chains of Tyr2 within E2lipD and Tyr148 within PSBD are sufficiently exposed to be capable of interacting with graphene without substantial disruption of the E2lipD or PSBD structures. A combination of such π-π interactions with van der Waals forces would permit adsorption of E2 complexes with retention of supramolecular structure. If the E2-graphene interaction involves solely or mainly the linkers and peripheral domains, E2lipD and PSBD (Figure 1), on one side of the complex then the E2 catalytic domain core assembly is even less likely to be disrupted. Additionally, even if the peripheral domains contacting graphene were partially or fully unfolded, the core catalytic domain scaffold and peripheral domains exposed to solvent would be likely to remain folded. Evidently the interaction permits E2 complex mobility over the graphene surface, compatible with our observations that E2 complexes form network-, cellular- and labyrinth-type patterns on graphenic surfaces and that an AFM tip at moderate scanning speeds can swipe clean E2-graphene. The apparent height reduction of E2 complexes on graphene, as indicated by the difference between a diameter of about 17 nm measured by TEM and a height of 10-11 nm measured by AFM, may reflect crumpling of the inter-domain linkers (Figure 1) on the face of the complex that interacts with graphene. Due to the symmetry of the E2 complex, the nature of the E2-graphene interaction is probably largely uniform across the E2 complex population, in line with the consistent aspect of E2 complexes presented in the high resolution AFM images (Figure 3), and explaining the relatively homogeneous monolayer coverage of graphene (Figure 2). On the hydrophilic SiO_2 and sapphire surfaces, the severe height reduction to ~4 nm indicates that the E2 complex experiences substantial disruption, potentially including at least partial disassembly of the core catalytic domain scaffold.

2.3. E2-graphene as a biosensing platform

For sensing it is crucial to demonstrate that E2-graphene can bind a target molecule specifically without activity loss. We therefore tested E1, one of E2's physiological partner enzymes, in conjunction with E2-graphene. Before assays, E1 was incubated with its natural cofactor, thiamine pyrophosphate (TPP). TPP facilitates the carbon-carbon bond cleavage involved in E1-catalysed oxidative decarboxylation, in this case the carbon-carbon bond adjacent to the carbonyl group of the E1 substrate 3-methyl-2-oxopentanoate.

E1 binding to E2-graphene was demonstrated through a combination of AFM imaging (Figure 4(a)) and field effect transistor (FET) transconductance measurements (Figure 4(b), and SI). Figure 4(a) compares the morphology of E2-graphene before (panel 1) and after (panel 2) early stage incubation with E1 (i.e. 10 minutes incubation, compared to 40 minutes incubation used in electrochemical assays); this shorter incubation allowed recognition of the targeted area, before E1 coverage completely obscures the E2 layer. The image after E1 incubation (panel 2) appears fuzzier and with increased coverage, while framed regions highlight differences due to bound E1 in easily recognizable areas. By comparing the height distributions derived from the images in panels 1 and 2 (see panel 3), after E1 incubation there is clear diminution of the counts in the lower region (which we attribute to the AFM tip probing regions between neighboring E2 complexes); instead, the distribution shifts towards greater height, directly demonstrating E1 presence on E2-graphene. We also followed how FET transconductance against electrochemical gate voltage changes with E1 binding until saturation is achieved. E2-graphene was successively incubated with increasingly concentrated E1 solutions, each incubation being followed by a transconductance measurement (see Experimental Section). The transconductance curves shifted

neutrality point towards higher gate voltages and broadened considerably with E1 accumulation, until saturation (Figure 4(b)). This is consistent with a decrease in gating efficiency of the electrolyte due to changes in dielectric constant of the electrical double layer at the solid-liquid interface rather than a direct charge transfer effect due to E1; similar behavior was observed by Chen *et al*.[63] This conclusion is supported by opposite and different tendencies obtained by testing for both PBS effects and E2 binding, respectively, on the graphene transconductance vs. gate voltage curves (see further discussion in SI and Figures S12 and S13).

We then tested the electrochemical activity of bound E1 by using E2-graphene as an electrode (see Experimental Section). We used cyclic voltammetry (CV) and chronoamperometry to monitor E1-catalysed decarboxylation of 3-methyl-2-oxopentanoate to 3-methyl-4-hydroxy-butyl, employing 2,6-dichlorophenol indophenol (DCPIP) as artificial electron acceptor (mediator) to complete the redox cycle (Figure 4(c)). The subsequent steps in the physiological reaction sequence of a complete E1-E2-E3-lipoate ligase system would be lipoylation of TPP-E1-3-methyl-4-hydroxy-butyl (where TPP is E1's coenzyme) by lipoamide-E2 followed by release from TPP of 3-methyl-butanal-dihydrolipoamide-E2 and then reaction with coenzyme A (CoA) to form 3-methyl-butyl-CoA. Here, however, the E1 reaction is decoupled: there is neither lipoic acid nor lipoate ligase in the reaction mixture, both of which are required to form lipoamide-E2, and so E1-catalyzed decarboxylation of 3-methyl-2-oxopentanoate is the only enzymatic reaction taking place, with DCPIP as final electron acceptor.

Both bare graphene and E2-graphene electrodes are low noise, with featureless and low capacitive backgrounds in the absence of DCPIP (Figure 4(d)); this promotes high signal-to-noise

detection. When DCPIP mediator was added, the bare graphene electrode produced a voltammogram reflecting the redox process of DCPIP (Figure 4(d) and SI, Figure S14 (a)-(c)). Further, when E1 substrate, 3-methyl-2-oxopentanoate, was added to an electrochemical cell containing E1-E2-graphene electrode and DCPIP, the DCPIP-mediated redox process intensified with increasing E1 substrate concentration, clearly demonstrating bioelectrocatalysis (Figure 4(d)). Figure S14 shows a full set of voltammograms, spanning a large substrate concentration range: sensitivity is higher at lower E1 substrate concentrations, between 10^{-9} M and 10^{-6} M, followed by saturation towards 10^{-4} M substrate. Similar kinetic behavior was observed across several enzyme/graphene samples and a range of DCPIP concentrations (from 10 μM to 100 μM) (Figure S14 (a)-(c)). Across about 15 experiments, the catalytic current was seen to increase over this E1 substrate concentration range by between 50% and 150% relative to the base-line DCPIP current. Each E1-E2-graphene electrode was subjected to measurements over a period of several hours (up to 8 hours) at room temperature, retaining activity for this period. Control experiments (see SI, Figure S18) confirmed the absence of increased catalysis at the E2-graphene platform in the presence of DCPIP and E1 substrate, but, critically, without E1. No increase in activity was detected also when adding E1 substrate to the system containing bare, unfunctionalized graphene (i.e. without both E1 and E2) and DCPIP. These all confirmed that increased activity after E1 substrate addition occurs only when E1 adsorbs onto the E2-graphene platform.

The E1-derived origin of the additional current was confirmed by chronoamperometry (conducted in a droplet configuration, see Experimental; raw data in SI, Figure S16), in which current change with time is tracked as a function of increasing E1 substrate concentration at fixed potential (here, 0.25 V applied to graphene vs. silver reference electrode). Amperometry-derived

enzyme kinetics match closely CV-derived kinetics (Figure 4(e)). Overall, the kinetics could be fitted with a relationship of the $I = A/(1+(B/[S])^n)$ type, yielding a sub-linear value of $n = 0.31 \pm 0.05$ and $B = 1.45 (\pm 0.72) \times 10^{-8}$ M for the chronoamperometric data, and $n = 0.3 \pm 0.016$ and $B = 7.45 (\pm 1.3) \times 10^{-8}$ M for the (CV)-derived data, indicating non-Michaelis-Menten dependence for E1 activity. The kinetics approach Michaelis-Menten behavior at the higher E1 substrate concentrations (roughly 10^{-5} M and above), but deviate from Michaelis-Menten behavior at the lower end of the E1 substrate concentration range (SI, Figure S17 and Table S1). Further experiments will be needed to determine the cause of the deviation from Michaelis-Menten behavior.

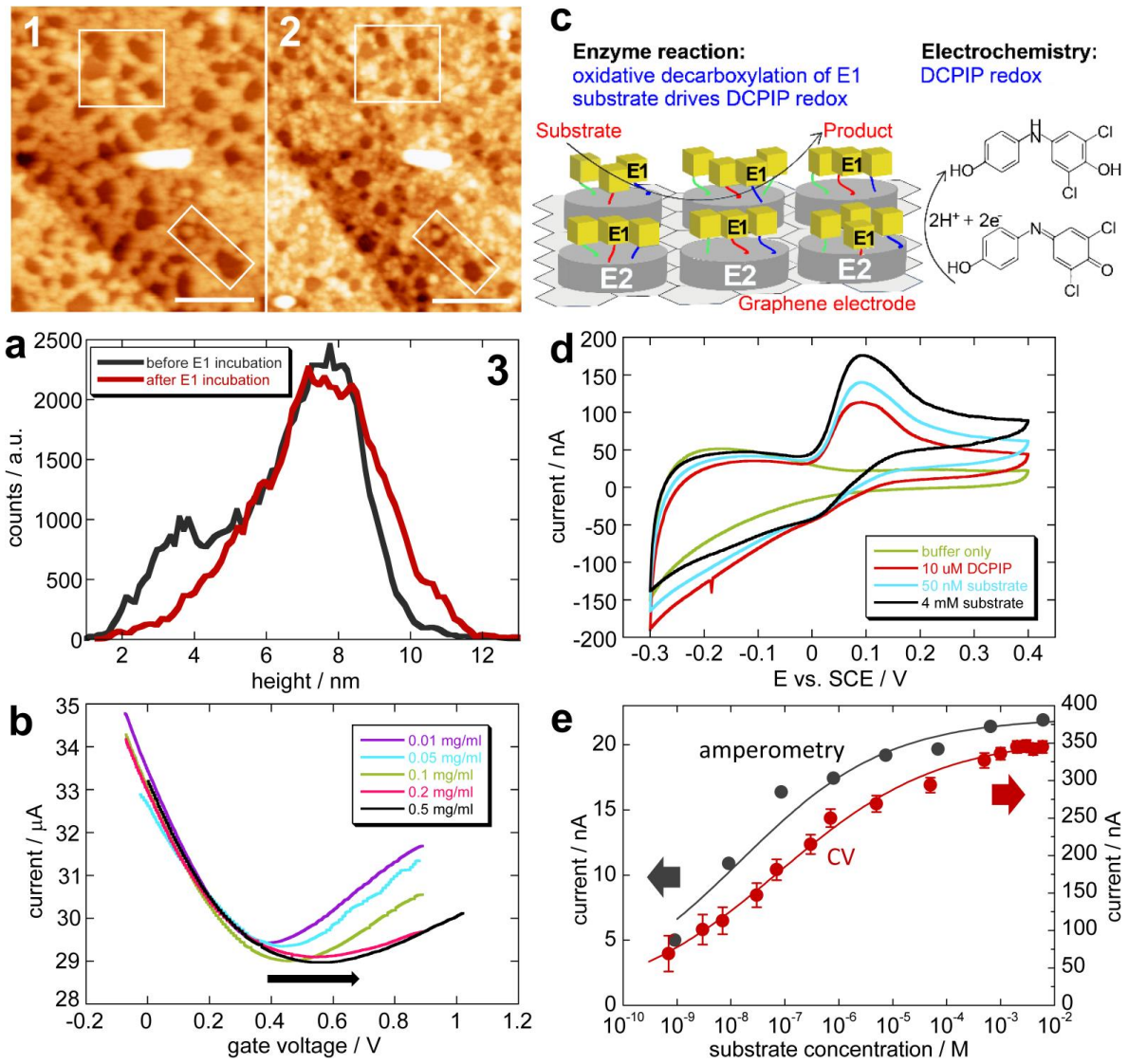

Figure 4. E2 complexes assemble on graphene to form a bio-platform on which target molecules can bind with retention of activity. E2-graphene is shown binding E1, E2's natural protein partner, by AFM and FET transconductance measurements. Cyclic voltammetry (CV) and chronoamperometry are used to demonstrate E1 activity after binding to E2-graphene. (a) "Before" and "after" AFM (tapping mode in air) of same region: E2-graphene (panel 1), and E1-E2-graphene (panel 2) after 10 minutes incubation of E2-graphene with 0.33 mg/ml E1 solution. Scale bars: 200 nm. Panel 3: height distributions before (black) and after (red) E1 early stage incubation,

as determined from the images in panels 1 and 2, respectively. (b) E1 attachment to E2-graphene is demonstrated *via* changes of FET transconductance against electrochemical gate voltage after E2-graphene incubation with E1 solutions of different concentrations (see Experimental Section, SI). (c) Enzymatic and electrochemical reaction schematics. (d) Cyclic voltammogram (scan rate 0.03 V s^{-1}) recorded after E1 immobilization on E2-graphene electrodes, in buffer only (olive), after adding 10 μM DCPIP (red), and after additions of 3-methyl-2-oxopentanoate of final concentrations 50 nM (turquoise) and 4 mM (black). A full set of CV curves is shown in SI, Figure S14 (a). (e) Enzyme kinetics derived from both chronoamperometry and CV from data obtained at 100 μM DCPIP (voltammograms shown in Figure S14 (c)). At each substrate concentration, the chronoamperometric current plateau value (Figure S16) was used.

There was no E1 activity on bare graphene electrodes, with and without mediator, demonstrating that E1 adsorbed directly onto graphene does not retain detectable activity. Importantly, there was no E1 activity when E1 was incubated on bovine serum albumin (BSA)-graphene electrodes (SI, Figure S19), showing either that E1 does not bind to BSA-graphene or that it binds non-productively; hence a non-specific (generic) protein spacer between E1 and graphene does not result in detectable E1 activity, highlighting the essential role of E2 in mediating biorecognition. It is reasonable to assume that E1-E2 interaction occurs via the physiological binding site, E2 PSBD (Figure 1). Preservation of E1 activity on E2-graphene platforms is an important result as binding to surfaces, especially hydrophobic surfaces such as bare graphene, often impairs protein function; in previous examples, the relatively robust protein concanavalin A[23] underwent almost complete loss of function upon adsorption onto graphene, and horseradish peroxidase[64] lost about 75% of its activity upon interaction with a graphenic material. As noted at the end of section 2.2,

however, IgG retains structure and function upon adsorption onto graphene,[60] and BSA is predicted by simulation also to retain its structure upon adsorption onto graphene.[61] Hence proteins display varying behavior upon direct interaction with graphene. Our results suggest that E2 complexes function as large footprint bridges that promote protein-surface interaction with retention of function. This is similar to the improvement brought about by tripodal linkers with large footprints[24] compared to monopodal ones, but with the advantages described above and shown further below of specificity and enhanced functionality and versatility.

The E1-E2-graphene system exhibits a very low detection limit, below 10^{-8} M substrate concentration, and a wide dynamic range spanning six orders of magnitude of substrate concentration. This is amongst the lowest detection limits encountered in biosensing with carbon-based systems.[15,17] E2-graphene performance contrasts strongly with E2-glassy carbon, where virtually no E1 activity was detected (data not shown). This highlights the key role played by graphene in allowing immobilized E2 complexes to retain substantial structural integrity and, consequently, specific binding capability. This behavior is rooted not only in the E2-graphene interactions (in which van der Waals forces and π–π stacking could be prominent, as discussed in section 2.2), but it potentially reflects also the relationship with the microstructure of the material: graphene has a flat, sp^2-bonded surface, promoting a more ordered E2 monolayer coverage, while glassy carbon contains randomly oriented graphitic interwoven ribbons, with fullerene-like structure (i.e. containing buckled sheets with both sp^2 and sp^3 content) that could result in distortion of the E2 complexes. Furthermore, E1-E2-graphene shows a short response time, of about three seconds (SI, Figure S16) - an important characteristic for real time, *in vivo* detection.

E2 is not an electron transfer protein and therefore the E2 complex is a poor electron conductor. In general, the need for a mediator could be eliminated by engineering prosthetic groups such as haem and iron-sulfur clusters into the interior of the E2 complex to form an efficient electron transfer pathway across the complex. This should be feasible since haem C and iron-sulfur clusters, for example, can be coordinated by cysteine residues of proteins, and non-native cysteines have previously been incorporated into the E2 complex interior to allow E2 conjugation with maleimide-bearing compounds.[43] In this scenario, E2 complexes with both interior and exterior modifications would be assembled on graphene.

2.4. Towards a multifunctional bio-platform

Finally, we produced a platform that incorporates different variants of E2. Modifications to E2 can create new functionalities, for example by reversible denaturation and reassembly of mixed E2 monomers[44] or incorporation of non-native cysteines for conjugation to the interior[43] or exterior of the E2 complex.[45] Alternatively, sortase A-mediated modification has been used for decoration of E2 complexes with multiple different molecules including one or more of antibody, enzyme, DNA aptamer and dye.[38,39] Here, we labeled E2 monomers with fluorescein isothiocyanate (FITC) or a Ni-NTA-Atto red dye. FITC reacts with primary amines ($–NH_3^+$) found at polypeptide chain N-termini and in lysine side-chains. Ni-NTA-Atto red affinity labels the target protein via metal chelation by an N-terminal hexahistidine tag (we incorporated such a tag in E2 monomers for purification rather than recognition/labelling purposes).

To illustrate the potential for E2 to be employed in multiplexed scenarios, micro-stamping was used as a convenient procedure to realize spatially separate regions of the two E2 variants (FITC-

and Ni-NTA-Atto-labelled) on graphene, allowing visualization by confocal laser scanning microscopy (Figure 5). E2 complex transfer was achieved without chemical linkers such as have been used previously for protein micro-patterning on graphene.[65] FITC and Ni-NTA-Atto have emission fluorescence peaks at 520 and 576 nm, respectively, and their fluorescence was not quenched by the electronically gapless graphene. With typical biomolecule-based spacers between the fluorophore and graphene, fluorescence quenching is due to non-radiative decay; this decreases significantly for sizeable spacer thicknesses,[66] as provided by E2 complexes which prevent FITC or Ni-NTA-Atto direct contact with graphene and which permit multiple FITC or Ni-NTA-Atto copies per complex. Ni-NTA-Atto-modified E2 complexes were stamped first and visualized at 488 nm excitation with a LP560 filter, which allowed collection of emitted light above 560 nm (Figure 5(a)). FITC-labelled E2 lines were stamped next, above the Ni-NTA-Atto-E2 lines but at a different angle. FITC-E2 was then visualized at 488 nm excitation with a BP505-530 emission filter, which allowed collection of emitted light between 505 and 530 nm (Figure 5(b). The whole pattern was revealed using a combination of red and green filters (Figure 5(c)), while AFM images show that the CVD graphene is present around the patterned E2 lines.

Better protein locational control and potentially decreased destruction risk for the underlying graphene may be achieved by more complex methods for E2 transfer than micro-stamping, such as E2 complex specific binding on appropriately functionalized graphene. In future work, we will evaluate the comparative advantages, in complexity and performance, of both strategies. Nevertheless, this first example of transfer of different variants of E2 complexes on graphene is an initial step towards creation of multiplexed, multi-functional devices. Surfaces in such devices

could have multiplexed chemical/biochemical micro-patterns where E2 complexes with different functionalities are controllably transferred to build multiple functionalities on one platform.[67]

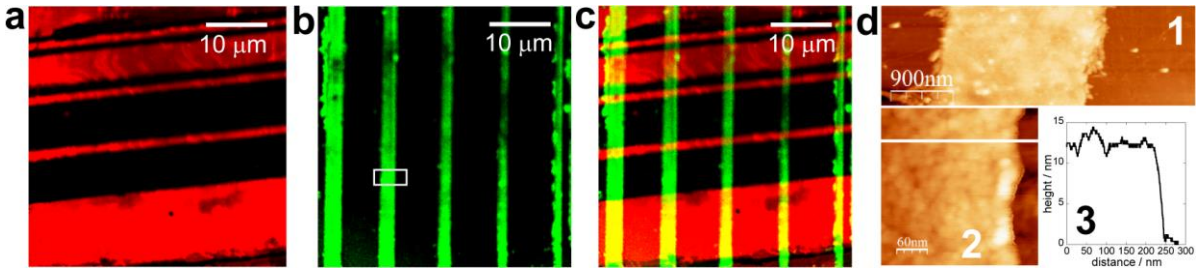

Figure 5. Multiplexing different types of E2 complexes on CVD graphene. (a) Ni-NTA-Atto-modified E2 complexes visualized at 488 nm excitation with a LP560 filter, which allowed collection of emitted light above 560 nm. (b) Lines of FITC-labelled E2 complexes visualized at 488 nm excitation with a BP505-530 emission filter, which allowed collection of emitted light between 505 and 530 nm. (c) The whole pattern was revealed using a combination of red and green filters. (d) AFM images (panels 1 and 2) and topographic profile (panel 3) showing the stamped patterns of E2 complexes on top of, and surrounded by, CVD graphene (easily identifiable by the presence of characteristic domain boundaries within the graphene film). Panel 1 corresponds to the framed area from image (b), while a zoom in this line pattern area (panel 2) shows globular units compatible in lateral dimension with E2 complexes.

3. Conclusion

We have introduced a new bio-platform that combines versatile, self-assembling E2 protein complexes with graphene. E2 complexes are robust and their customizability means that the E2-graphene platform can be adapted to multiple applications. Monolayer graphene (conveniently obtained in large areas and on a variety of substrates by CVD methods) provides a surface that is

sufficiently uniform and chemically simple to allow E2 complexes to directly self-assemble on it while retaining a supramolecular structure and ability to bind specifically to other enzymes without loss of enzyme function (here, tested with E1, E2's physiological partner). These capabilities are not replicated when E2 complexes are used with standard electrochemical electrodes such as glassy carbon, highlighting the advantages of graphene when interfacing these supramolecular complexes with the solid state. This is the first use of E2 for solid state sensing: we have shown that E2-graphene can detect E1 activity at substrate concentrations below 10^{-8} M, and that platforms can be made with defined patterns of different types of E2 complexes. Since the E2-graphene interaction is non-covalent, the graphene π–electron system is maintained and hence so are the numerous advantageous properties of graphene that derive from this electron system (including the capability of E2-graphene to be used in a field-effect transistor sensing configuration, which could be exploited in future iterations of this work).

Moving beyond this proof-of-principle study, the E2-graphene bio-platform can be customized by modifying the E2 subunits. Modified E2 complexes can be used for sensing,[39] catalysis,[38,39] encapsulation,[41,46] display/targeting/delivery,[40,43,68,69] switching,[46,47,70] imaging,[47] synthesis,[42] or a combination of one or more of these. The customization capacity of E2 and graphene means that the E2-graphene platform has considerable versatility and potential utility, for example for sensing a wide range of analytes, with the potential for greater functionality through multiplexing. The versatility of the E2-graphene platform increases further still when it is recognized that OADHCs are found in a huge range of organisms including aerobic bacteria and eukarya, providing a pool of E2 complexes encompassing a range of physico-chemical and biochemical characteristics such as number of component monomers, thermal stability, pH optimum, and charge distribution. We

will next interface graphene with further modified E2 complexes; interior modification to provide rapid electron transfer pathways ("internal wiring") through the E2 complex will be combined with exterior decoration of E2 complexes, for example with anti-microbial peptides to create an E2-graphene platform for sensing of bacterial pathogens.

4. Experimental Section

Expression and purification of E1 and E2. Recombinant *Thermoplasma acidophilum* E2 and E1 were purified via Ni^{2+}-affinity chromatography, as described previously,[37] dialysed into half strength phosphate buffered saline (PBS), pH 7.4 and stored at 4 °C until further use. Protein concentration was estimated by measuring absorbance at 280 nm in 6 M guanidine-HCl. E2 complex assembly was induced by incubating E2 monomers at 55 °C for 10 min; assembly into complexes was confirmed by dynamic light scattering and analytical ultracentrifugation and cryo-EM (SI). Prior to activity assays, E1 was incubated with its natural cofactor thiamine pyrophosphate (TPP, 0.2 mM) in the presence of 2 mM $MgCl_2$ at 55 °C for 10 min to allow TPP binding to E1.

E2 complex functionalization of graphene surfaces. All surfaces were incubated with E2 complexes from 0.1 mg/ml stock solution (incubation times described in main text), then rinsed with PBS to remove excess E2 complexes, or with deionized water when performing AFM in air. Reproducibility of coverage was about ± 10%, based on partitioning height in ten different AFM images about a threshold value and then summing areas above and below that value. HOPG research grade with 0.8° ± 0.2° mosaic spread (SPI), as opposed to a lower quality of graphite, gave good reproducibility and uniformity across the surface. For TEM, E2 complexes were incubated on graphene membranes, followed by negative staining with uranyl acetate for contour enhancement.

AFM scanning conditions. Imaging of E2 complexes and measurement of apparent heights was performed in tapping mode in air on a MFP-3D Asylum microscope, with Si cantilevers (Olympus AC240TS, ~ 2 N/m spring constant, and ~ 73 kHz resonance frequency), in the regime of attractive average forces (phase > 90°) and with the smallest oscillation amplitude attainable (~ 5 nm) to

minimize dynamic forces and increase sensitivity to short range forces (SI). High resolution imaging of E2 complex structure in air was obtained by decreasing the setpoint (i.e. the measured-to-free amplitude ratio) until improved resolution was obtained in both topographic and phase images; or by working in liquid (on a Cypher microscope) with stiff, short cantilevers (BioLever Fast, 9 μm, 0.1 N/m, 1.5 MHz from Olympus) to ensure small oscillation amplitudes, and without protein fixation. See also SI.

Electrochemical measurements of enzyme activity. Cyclic voltammetry (CV) was carried out in a purpose built three-electrode cell (volume ~4 cm^3) containing glassy carbon counter, KCl-saturated calomel reference (SCE, Radiometer, Copenhagen) and CVD graphene (~12 mm^2) or glassy carbon (3 mm diameter) as working electrode. The reaction buffer contained PBS, pH 7.4, and 2 mM $MgCl_2$, while concentrations of DCPIP spanning from 10 to 100 μM were used across various experiments. 40 μl of EDTA was added to the reaction solution as a metal chelator, followed by 40 μl of $MgCl_2$ to mop up any EDTA in the final solution. For electrochemistry experiments, E1 was incubated on E2-graphene from 0.33 mg/ml stock solution typically for 40 minutes. Experiments on $n \geq 15$ E1-E2-graphene samples resulted in very similar trends; five scans were taken at each substrate concentration, reproducibility being obtained usually after the second scan. The CV-derived E1 kinetics were obtained from the anodic current measured at 80 mV vs. SCE (after subtracting the DCPIP signal from it, and correcting for the slight increase of the non-Faradaic contribution after sequential substrate additions).

Chronoamperometry was performed in a droplet configuration: a silicone rubber reservoir (~50 μl) was formed around the graphene active area (~12 mm^2), after which graphene was incubated with E2 and then E1, as for cyclic voltammetry. 20 μl of the final solution, including DCPIP, covered E1-E2-graphene, and 1-2 μl of substrate of increasing stock concentration was added to

the droplet. Silver (0.3 mm diameter) and platinum (0.3 mm diameter) wires, 2 mm distance apart and 1.5 mm immersion depth, were used as quasi-reference and auxiliary electrodes, respectively (see also SI, Figure S14). A potential of 0.25 V vs. Ag was applied, while the chronoamperometric current was measured after sequential additions of 2 μl substrate to 20 μl drop of PBS with 100 μM DCPIP as mediator (see SI, Figure S15). This current was used for determining the E1 kinetics shown in Figure 4(e), where the increase in droplet volume was considered when determining final substrate concentrations. Controls involving addition of just PBS to the droplet did not trigger an amperometric signal. Chronoamperometry in volumes as used for CV gave no measurable current without stirring, and a low signal-to-noise ratio with stirring.

FET with liquid gate for detecting E1 attachment on E2-graphene. The transistor consisted of CVD monolayer graphene (~ 12 mm^2) dry-transferred onto a SiO_2(300nm)/Si substrate (see SI), with deposited metal contacts (10 nm Ti/ 50 nm Au), silicone rubber or solid PDMS defining a reservoir (~ 50 μl) protecting the electrodes and leaving just graphene exposed to analyte; and a silver wire (0.3 mm diameter) as gate electrode in PBS (of various dilution factors). The source-drain voltage was V_{sd} = 0.2 V for a length of channel of about 3 mm. E2 complexes (0.1 mg/ml solution) were first incubated for 10 minutes, the surface was washed with PBS, then 20 μl drops of increasing concentration (from 0.01 mg/ml to 1 mg/ml) of E1 in PBS were successively placed in the reservoir and incubated for 10 minutes. After each incubation, the graphene surface was rinsed with PBS to remove weakly attached proteins, and 40 μl of fresh diluted PBS (Debye length ~ 3.5 nm) was then put as electrolyte in the reservoir to create the double layer required for transconductance measurements. Control experiments assessing effect of PBS, as well as E2 attachment to graphene are described in SI.

Fluorescent labelling of E2. E2 complexe (1 mg/ml) was labelled using fluorescein isothiocyanate (FITC, 1 mg/ml in DMF, Sigma) or Ni-NTA-Atto 550 (Sigma) following the manufacturer's instructions. Samples were dialysed against half-strength PBS, pH 7.4 at 4 °C to remove any unbound fluorescent label.

ASSOCIATED CONTENT

Supporting Information (SI). 1. Protein purification methods. 2. Distribution of polar/non-polar sequences in the *T. acidophilum* E2 monomer. 3. Cryo-EM images of the assembled 60-mer E2 nanoparticle of *T. acidophilum* 2-OADHC. 4. Quantitative characterization of an E2 complex biomolecular monolayer formed on graphenic surfaces. 5. Graphene growth by CVD; Transfer protocol; Assessment of graphene quality. 6. E2 monomer vs. E2 complex attachment on graphenic surfaces. 7. Self-assembly of E2 nanoparticles on various graphenic surfaces: (i) drying-mediated, and (ii) assembly from liquid phase. 8. Morphology of E2 nanoparticles on various surfaces; Real vs. apparent height. 9. Field-effect transistor experiments assessing E2 and E1 attachment. 10. Supporting and control electrochemistry experiments: (i) Cyclic voltammetry and chronoamperometry of E1 bound to E2-graphene; (ii) Control experiments: bare graphene; E2-graphene; E1 on BSA-graphene; (iii) DCPIP redox processes at CVD graphene. 11. Microcontact printing/stamping protocol on graphene surfaces.

This material is available free of charge via the Internet at http://pubs.acs.org.

AUTHOR INFORMATION

Corresponding Author

*Adelina Ilie, email: a.ilie@bath.ac.uk, *Stefan Bagby, email: bsssb@bath.ac.uk

Author Contributions

‡ AA and MGP contributed equally to this research. AI, SB, MGP and AU designed the overall work program. AA performed surface functionalization, atomic force microscopy, electrochemistry experiments, liquid-gated FET fabrication and measurements, graphene film growth/transfer, and related analysis, micro-stamping and laser scanned confocal microscopy; while MGP performed protein expression and purification, solution assays, dynamic light scattering, protein labelling and modification, and participated in electrochemistry experiments. FM assisted with the electrochemistry experiments and their interpretation. AI and SB supervised the research and wrote the paper, while all authors provided comments and agreed with the final form of the manuscript.

ACKNOWLEDGMENTS

This work was supported by a Science and Innovation Award (EP/G036101/1) from the United Kingdom Engineering and Physical Sciences Research Council and a grant from the University of Bath EPSRC Delivery Fund (EDF44). AA gratefully acknowledges a studentship from the Ministry of Higher Education, Saudi Arabia, while MGP gratefully acknowledges receipt of a UNESCO-L'Oréal FWIS Fellowship. The authors also thank Prof. Richard Henderson (MRC Laboratory of Molecular Biology, Cambridge) for the cryo-EM images of E2 complexes, and Ursula Potter and Adrian Rogers (University of Bath) for their assistance with the TEM examinations and confocal laser scanning microscopy, respectively.

REFERENCES

(1) Li, C.; Adamcik, J.; Mezzenga, R. Biodegradable Nanocomposites of Amyloid Fibrils and Graphene with Shape-Memory and Enzyme-Sensing Properties. *Nat. Nanotechnol.* **2012,** *7* (7), 421-427.

(2) Naik, R. R.; Stringer, S. J.; Agarwal, G.; Jones, S. E.; Stone, M. O. Biomimetic Synthesis and Patterning of Silver Nanoparticles. *Nat. Mater.* **2002,** *1* (3), 169-172.

(3) Mao, C. B.; Solis, D. J.; Reiss, B. D.; Kottmann, S. T.; Sweeney, R. Y.; Hayhurst, A.; Georgiou, G.; Iverson, B.; Belcher, A. M. Virus-Based Toolkit for the Directed Synthesis of Magnetic and Semiconducting Nanowires. *Science* **2004,** *303* (5655), 213-217.

(4) Goede, K.; Busch, P.; Grundmann, M. Binding Specificity of a Peptide on Semiconductor Surfaces. *Nano Lett.* **2004,** *4* (11), 2115-2120.

(5) Chiu, C. C.; Maher, M. C.; Dieckmann, G. R.; Nielsen, S. O. Molecular Dynamics Study of a Carbon Nanotube Binding Reversible Cyclic Peptide. *ACS Nano* **2010,** *4* (5), 2539-2546.

(6) Kim, Y. H.; Campbell, E.; Yu, J.; Minteer, S. D.; Banta, S. Complete Oxidation of Methanol in Biobattery Devices Using a Hydrogel Created from Three Modified Dehydrogenases. *Angew. Chem. Int. Ed.* **2013,** *52* (5), 1437-1440.

(7) Sato, K.; Anzai, J.-i. Dendrimers in Layer-by-Layer Assemblies: Synthesis and Applications. *Molecules* **2013,** *18* (7), 8440-8460.

(8) Milton, R. D.; Hickey, D. P.; Abdellaoui, S.; Lim, K.; Wu, F.; Tan, B.; Minteer, S. D. Rational Design of Quinones for High Power Density Biofuel Cells. *Chem. Sci.* **2015,** *6* (8), 4867-4875.

(9) Hickey, D. P.; Reid, R. C.; Milton, R. D.; Minteer, S. D. A Self-Powered Amperometric Lactate Biosensor Based on Lactate Oxidase Immobilized in Dimethylferrocene-Modified Lpei. *Biosens. Bioelectron.* **2016,** *77*, 26-31.

(10) Meredith, S.; Xu, S.; Meredith, M. T.; Minteer, S. D. Hydrophobic Salt-Modified Nafion for Enzyme Immobilization and Stabilization. *J. Visualized Exp.* **2012,** (65), 3949.

(11) Schuster, B.; Sleytr, U. B. Biomimetic Interfaces Based on S-Layer Proteins, Lipid Membranes and Functional Biomolecules. *J. R. Soc., Interface* **2014,** *11* (96), 20140232.

(12) Su, W. W.; Han, Z. Self-Assembled Synthetic Protein Scaffolds: Biosynthesis and Applications. *ECS Trans.* **2013,** *50* (28), 23-29.

(13) Feifel, S. C.; Kapp, A.; Ludwig, R.; Lisdat, F. Nanobiomolecular Multiprotein Clusters on Electrodes for the Formation of a Switchable Cascadic Reaction Scheme. *Angew. Chem. Int. Ed.* **2014,** *53* (22), 5676-5679.

(14) Schedin, F.; Geim, A. K.; Morozov, S. V.; Hill, E. W.; Blake, P.; Katsnelson, M. I.; Novoselov, K. S. Detection of Individual Gas Molecules Adsorbed on Graphene. *Nat. Mater.* **2007,** *6* (9), 652-655.

(15) Kuila, T.; Bose, S.; Khanra, P.; Mishra, A. K.; Kim, N. H.; Lee, J. H. Recent Advances in Graphene-Based Biosensors. *Biosens. Bioelectron.* **2011,** *26* (12), 4637-4648.

(16) Hess, L. H.; Jansen, M.; Maybeck, V.; Hauf, M. V.; Seifert, M.; Stutzmann, M.; Sharp, I. D.; Offenhausser, A.; Garrido, J. A. Graphene Transistor Arrays for Recording Action Potentials from Electrogenic Cells. *Adv. Mater.* **2011,** *23* (43), 5045-5049.

(17) Yang, C.; Denno, M. E.; Pyakurel, P.; Venton, B. J. Recent Trends in Carbon Nanomaterial-Based Electrochemical Sensors for Biomolecules: A Review. *Anal. Chim. Acta* **2015,** *887*, 17-37.

(18) Bai, H.; Xu, Y. X.; Zhao, L.; Li, C.; Shi, G. Q. Non-Covalent Functionalization of Graphene Sheets by Sulfonated Polyaniline. *Chem. Commun.* **2009,** (13), 1667-1669.

(19) Cui, Y.; Kim, S. N.; Jones, S. E.; Wissler, L. L.; Naik, R. R.; McAlpine, M. C. Chemical Functionalization of Graphene Enabled by Phage Displayed Peptides. *Nano Lett.* **2010,** *10* (11), 4559-4565.

(20) Kim, S. N.; Kuang, Z. F.; Slocik, J. M.; Jones, S. E.; Cui, Y.; Farmer, B. L.; McAlpine, M. C.; Naik, R. R. Preferential Binding of Peptides to Graphene Edges and Planes. *J. Am. Chem. Soc.* **2011,** *133* (37), 14480-14483.

(21) Mannoor, M. S.; Tao, H.; Clayton, J. D.; Sengupta, A.; Kaplan, D. L.; Naik, R. R.; Verma, N.; Omenetto, F. G.; McAlpine, M. C. Graphene-Based Wireless Bacteria Detection on Tooth Enamel. *Nat. Commun.* **2012,** *3*, 763.

(22) Khatayevich, D.; Page, T.; Gresswell, C.; Hayamizu, Y.; Grady, W.; Sarikaya, M. Selective Detection of Target Proteins by Peptide-Enabled Graphene Biosensor. *Small* **2014,** *10* (8), 1505-1513.

(23) Alava, T.; Mann, J. A.; Theodore, C.; Benitez, J. J.; Dichtel, W. R.; Parpia, J. M.; Craighead, H. G. Control of the Graphene-Protein Interface Is Required to Preserve Adsorbed Protein Function. *Anal. Chem.* **2013,** *85* (5), 2754-2759.

(24) Mann, J. A.; Dichtel, W. R. Improving the Binding Characteristics of Tripodal Compounds on Single Layer Graphene. *ACS Nano* **2013,** *7* (8), 7193-7199.

(25) Feifel, S. C.; Lokstein, H.; Hejazi, M.; Zouni, A.; Lisdat, F. Unidirectional Photocurrent of Photosystem I on Π-System-Modified Graphene Electrodes: Nanobionic Approaches for the Construction of Photobiohybrid Systems. *Langmuir* **2015,** *31* (38), 10590-10598.

(26) Green, N. S.; Norton, M. L. Interactions of DNA with Graphene and Sensing Applications of Graphene Field-Effect Transistor Devices: A Review. *Anal. Chim. Acta* **2015,** *853* (0), 127-142.

(27) Lu, L. M.; Qiu, X. L.; Zhang, X. B.; Shen, G. L.; Tan, W. H.; Yu, R. Q. Supramolecular Assembly of Enzyme on Functionalized Graphene for Electrochemical Biosensing. *Biosens. Bioelectron.* **2013,** *45*, 102-107.

(28) Lerner, M. B.; Matsunaga, F.; Han, G. H.; Hong, S. J.; Xi, J.; Crook, A.; Perez-Aguilar, J. M.; Park, Y. W.; Saven, J. G.; Liu, R. Y.; Johnson, A. T. C. Scalable Production of Highly Sensitive Nanosensors Based on Graphene Functionalized with a Designed G Protein-Coupled Receptor. *Nano Lett.* **2014,** *14* (5), 2709-2714.

(29) Hess, L. H.; Lyuleeva, A.; Blaschke, B. M.; Sachsenhauser, M.; Seifert, M.; Garrido, J. A.; Deubel, F. Graphene Transistors with Multifunctional Polymer Brushes for Biosensing Applications. *ACS Appl. Mater. Interfaces* **2014,** *6* (12), 9705-9710.

(30) Yang, W. R.; Ren, Q.; Wu, Y. N.; Morris, V. K.; Rey, A. A.; Braet, F.; Kwan, A. H.; Sunde, M. Surface Functionalization of Carbon Nanomaterials by Self-Assembling Hydrophobin Proteins. *Biopolymers* **2013,** *99* (1), 84-94.

(31) Perham, R. N. Swinging Arms and Swinging Domains in Multifunctional Enzymes: Catalytic Machines for Multistep Reactions. *Annu. Rev. Biochem.* **2000,** *69* (1), 961-1004.

(32) Milne, J. L. S.; Shi, D.; Rosenthal, P. B.; Sunshine, J. S.; Domingo, G. J.; Wu, X. W.; Brooks, B. R.; Perham, R. N.; Henderson, R.; Subramaniam, S. Molecular Architecture and Mechanism of an Icosahedral Pyruvate Dehydrogenase Complex: A Multifunctional Catalytic Machine. *EMBO J.* **2002,** *21* (21), 5587-5598.

(33) Frank, R. A. W.; Pratap, J. V.; Pei, X. Y.; Perham, R. N.; Luisi, B. F. The Molecular Origins of Specificity in the Assembly of a Multienzyme Complex. *Structure* **2005,** *13* (8), 1119-1130.

(34) Lessard, I. A. D.; Fuller, C.; Perham, R. N. Competitive Interaction of Component Enzymes with the Peripheral Subunit-Binding Domain of the Pyruvate Dehydrogenase Multienzyme Complex of Bacillus Stearothermophilus: Kinetic Analysis Using Surface Plasmon Resonance Detection. *Biochemistry* **1996,** *35* (51), 16863-16870.

(35) Izard, T.; Aevarsson, A.; Allen, M. D.; Westphal, A. H.; Perham, R. N.; de Kok, A.; Hol, W. G. J. Principles of Quasi-Equivalence and Euclidean Geometry Govern the Assembly of Cubic and Dodecahedral Cores of Pyruvate Dehydrogenase Complexes. *Proc. Natl. Acad. Sci. U. S. A.* **1999,** *96* (4), 1240-1245.

(36) Marrott, N. L.; Marshall, J. J. T.; Svergun, D. I.; Crennell, S. J.; Hough, D. W.; Danson, M. J.; van den Elsen, J. M. H. The Catalytic Core of an Archaeal 2-Oxoacid Dehydrogenase Multienzyme Complex Is a 42-Mer Protein Assembly. *FEBS J.* **2012,** *279* (5), 713-723.

(37) Heath, C.; Posner, M. G.; Aass, H. C.; Upadhyay, A.; Scott, D. J.; Hough, D. W.; Danson, M. J. The 2-Oxoacid Dehydrogenase Multi-Enzyme Complex of the Archaeon Thermoplasma Acidophilum - Recombinant Expression, Assembly and Characterization. *FEBS J.* **2007,** *274* (20), 5406-5415.

(38) Chen, Q.; Sun, Q.; Molino, N. M.; Wang, S.-W.; Boder, E. T.; Chen, W. Sortase a-Mediated Multi-Functionalization of Protein Nanoparticles. *Chem. Commun.* **2015,** *51* (60), 12107-12110.

(39) Sun, Q.; Chen, Q.; Blackstock, D.; Chen, W. Post-Translational Modification of Bionanoparticles as a Modular Platform for Biosensor Assembly. *ACS Nano* **2015,** *9* (8), 8554-8561.

(40) Ren, D.; Kratz, F.; Wang, S.-W. Protein Nanocapsules Containing Doxorubicin as a pH-Responsive Delivery System. *Small* **2011,** *7* (8), 1051-1060.

(41) Ren, D.; Dalmau, M.; Randall, A.; Shindel, M. M.; Baldi, P.; Wang, S.-W. Biomimetic Design of Protein Nanomaterials for Hydrophobic Molecular Transport. *Adv. Funct. Mater.* **2012,** *22* (15), 3170-3180.

(42) Peng, T.; Paramelle, D.; Sana, B.; Lee, C. F.; Lim, S. Designing Non-Native Iron-Binding Site on a Protein Cage for Biological Synthesis of Nanoparticles. *Small* **2014,** *10* (15), 3131-3138.

(43) Ren, D.; Kratz, F.; Wang, S.-W. Engineered Drug-Protein Nanoparticle Complexes for Folate Receptor Targeting. *Biochem. Eng. J.* **2014,** *89*, 33-41.

(44) Domingo, G. J.; Orru, S.; Perham, R. N. Multiple Display of Peptides and Proteins on a Macromolecular Scaffold Derived from a Multienzyme Complex. *J. Mol. Biol.* **2001,** *305* (2), 259-267.

(45) Molino, N. M.; Bilotkach, K.; Fraser, D. A.; Ren, D. M.; Wang, S. W. Complement Activation and Cell Uptake Responses toward Polymer-Functionalized Protein Nanocapsules. *Biomacromolecules* **2012,** *13* (4), 974-981.

(46) Dalmau, M.; Lim, S. R.; Wang, S. W. Design of a pH-Dependent Molecular Switch in a Caged Protein Platform. *Nano Lett.* **2009,** *9* (1), 160-166.

(47) Peng, T.; Lee, H.; Lim, S. Design of a Reversible Inversed pH-Responsive Caged Protein. *Biomater. Sci.* **2015,** *3* (4), 627-635.

(48) Bae, S.; Kim, H.; Lee, Y.; Xu, X.; Park, J.-S.; Zheng, Y.; Balakrishnan, J.; Lei, T.; Ri Kim, H.; Song, Y. I.; Kim, Y.-J.; Kim, K. S.; Ozyilmaz, B.; Ahn, J.-H.; Hong, B. H.; Iijima, S. Roll-to-Roll Production of 30-Inch Graphene Films for Transparent Electrodes. *Nat. Nanotechnol.* **2010,** *5* (8), 574-578.

(49) Lee, H.; Choi, T. K.; Lee, Y. B.; Cho, H. R.; Ghaffari, R.; Wang, L.; Choi, H. J.; Chung, T. D.; Lu, N.; Hyeon, T.; Choi, S. H.; Kim, D.-H. A Graphene-Based Electrochemical Device with Thermoresponsive Microneedles for Diabetes Monitoring and Therapy. *Nat. Nanotechnol.* **2016,** *11*, 566-572.

(50) Geim, A. K.; Novoselov, K. S. The Rise of Graphene. *Nat. Mater.* **2007,** *6* (3), 183-191.

(51) Garcia, R.; San Paulo, A. Attractive and Repulsive Tip-Sample Interaction Regimes in Tapping-Mode Atomic Force Microscopy. *Phys. Rev. B* **1999,** *60* (7), 4961-4967.

(52) Tamayo, J.; Humphris, A. D. L.; Miles, M. J. Piconewton Regime Dynamic Force Microscopy in Liquid. *Appl. Phys. Lett.* **2000,** *77* (4), 582-584.

(53) Brownson, D. A. C.; Banks, C. E. The Electrochemistry of CVD Graphene: Progress and Prospects. *Phys. Chem. Chem. Phys.* **2012,** *14* (23), 8264-8281.

(54) Li, W.; Tan, C.; Lowe, M. A.; Abruña, H. D.; Ralph, D. C. Electrochemistry of Individual Monolayer Graphene Sheets. *ACS Nano* **2011,** *5* (3), 2264-2270.

(55) van Hulst, N. F.; Garcia-Parajo, M. F.; Moers, M. H. P.; Veerman, J. A.; Ruiter, A. G. T. Near-Field Fluorescence Imaging of Genetic Material: Toward the Molecular Limit. *J. Struct. Biol.* **1997,** *119* (2), 222-231.

(56) Strack, G.; Nichols, R.; Atanassov, P.; Luckarift, H.; Johnson, G. Modification of Carbon Nanotube Electrodes with 1-Pyrenebutanoic Acid, Succinimidyl Ester for Enhanced Bioelectrocatalysis. In *Immobilization of Enzymes and Cells*, Guisan, J. M., Ed. Humana Press: **2013**; Chapter 14, pp 217-228.

(57) Rabani, E.; Reichman, D. R.; Geissler, P. L.; Brus, L. E. Drying-Mediated Self-Assembly of Nanoparticles. *Nature* **2003,** *426* (6964), 271-274.

(58) Stannard, A.; Martin, C. P.; Pauliac-Vaujour, E.; Moriarty, P.; Thiele, U. Dual-Scale Pattern Formation in Nanoparticle Assemblies. *J. Phys. Chem. C* **2008,** *112* (39), 15195-15203.

(59) Tang, J.; Ge, G.; Brus, L. E. Gas−Liquid−Solid Phase Transition Model for Two-Dimensional Nanocrystal Self-Assembly on Graphite. *J. Phys. Chem. B* **2002,** *106* (22), 5653-5658.

(60) Vilhena, J. G.; Dumitru, A. C.; Herruzo, E. T.; Mendieta-Moreno, J. I.; Garcia, R.; Serena, P. A.; Perez, R. Adsorption Orientations and Immunological Recognition of Antibodies on Graphene. *Nanoscale* **2016,** *8* (27), 13463-13475.

(61) Vilhena, J. G.; Rubio-Pereda, P.; Vellosillo, P.; Serena, P. A.; Pérez, R. Albumin (Bsa) Adsorption over Graphene in Aqueous Environment: Influence of Orientation, Adsorption Protocol, and Solvent Treatment. *Langmuir* **2016,** *32* (7), 1742-1755.

(62) Posner, Mareike G.; Upadhyay, A.; Crennell, Susan J.; Watson, Andrew J. A.; Dorus, S.; Danson, Michael J.; Bagby, S. Post-Translational Modification in the Archaea: Structural Characterization of Multi-Enzyme Complex Lipoylation. *Biochemical Journal* **2013,** *449* (2), 415-425.

(63) Chen, R. J.; Bangsaruntip, S.; Drouvalakis, K. A.; Wong Shi Kam, N.; Shim, M.; Li, Y.; Kim, W.; Utz, P. J.; Dai, H. Noncovalent Functionalization of Carbon Nanotubes for Highly Specific Electronic Biosensors. *P. Natl. Acad. Sci. U.S.A.* **2003,** *100* (9), 4984-4989.

(64) Zhang, J. L.; Zhang, F.; Yang, H. J.; Huang, X. L.; Liu, H.; Zhang, J. Y.; Guo, S. W. Graphene Oxide as a Matrix for Enzyme Immobilization. *Langmuir* **2010,** *26* (9), 6083-6085.

(65) Kodali, V. K.; Scrimgeour, J.; Kim, S.; Hankinson, J. H.; Carroll, K. M.; de Heer, W. A.; Berger, C.; Curtis, J. E. Nonperturbative Chemical Modification of Graphene for Protein Micropatterning. *Langmuir* **2011,** *27* (3), 863-865.

(66) Kasry, A.; Ardakani, A. A.; Tulevski, G. S.; Menges, B.; Copel, M.; Vyklicky, L. Highly Efficient Fluorescence Quenching with Graphene. *J. Phys. Chem. C* **2012,** *116* (4), 2858-2862.

(67) Didar, T. F.; Foudeh, A. M.; Tabrizian, M. Patterning Multiplex Protein Microarrays in a Single Microfluidic Channel. *Anal. Chem.* **2012,** *84* (2), 1012-1018.

(68) Molino, N. M.; Anderson, A. K. L.; Nelson, E. L.; Wang, S.-W. Biomimetic Protein Nanoparticles Facilitate Enhanced Dendritic Cell Activation and Cross-Presentation. *ACS Nano* **2013,** *7* (11), 9743-9752.

(69) Trovato, M.; Berardinis, P. D. Novel Antigen Delivery Systems. *World J. Virology* **2015,** *4* (3), 156-168.

(70) Peng, T.; Lim, S. Trimer-Based Design of pH-Responsive Protein Cage Results in Soluble Disassembled Structures. *Biomacromolecules* **2011,** *12* (9), 3131-3138.

Table of Contents Graphic